Sumpplementary of "Transport properties of Metallic Ruthenates: a DFT+DMFT investigation"

Xiaoyu Deng,[1] Kristjan Haule,[1] and Gabriel Kotliar[1]

[1] *Department of Physics and Astronomy, Rutgers University, Piscataway, New Jersey 08854, USA*

(Dated: May 25, 2016)

Appendix A: Computational details

The all-electron LDA plus dynamical mean field theory (LDA+DMFT) calculation with full charge-self-consistence is performed with an implementation described in Ref. 1, which is based on WIEN2k package[2]. We use projectors within a large (20eV) energy window to construct local orbitals, thus the oxygen orbitals hybridizing with the d orbitals are explicitly included. With such a large energy window the resulting d orbitals are very localized. This large energy window permits us to use the same interaction parameters for all the compounds considered. We treat t_{2g} dynamically with DMFT and all other states statically, and no states are eliminated in the calculations. The standard "double counting" scheme with fully localized form $\Sigma_{DC} = U(n_{imp} - 1/2) - \frac{1}{2}J(n_{imp} - 1)$ is used, where n_{imp} is the nominal occupancy of d-orbitals.

The interaction parameters are estimated by evaluating the Slater integrals within the localized orbitals assuming a screened Yukawa-form Coulomb potential $e^{-r/\lambda}/r$. Since a large energy window is used in our calculations, it is reasonable to set the Hubbard interaction to a fixed yet physical value by varying slightly the Thomas-Fermi screening length λ. Here we set $F^0 = 4.5$eV, a physical reasonable value. The corresponding λ varies in a narrow range [0.775, 0.8] Bohr radius, and the resulting Slater-integral $(F^2, F^4) \simeq (8.0, 6.5)$eV in all the ruthenates considered. Therefore we reach a uniform set of interaction parameters for all the ruthenates considered. In terms of Hubbard interaction U and Hund's coupling J, this set of parameters amounts to $(U, J) = (F^0, (F^2 + F^4)/14) \simeq (4.5, 1.0)$eV. It turns out these interaction parameters give quite accurate descriptions of various measured properties, as shown in the main text. We note that a large $J = 1.0$eV is necessary in our computational scheme to obtain a resistivity that has similar scale as the experimental measurements. This is seen in Fig.1, which shows that a reduced $J = 0.7$eV significantly underestimates the resistivity of $CaRuO_3$. This is consistent with the observation that ruthenates are typical Hund's metals where Hund's coupling J plays a major role in determining the correlation strength[3]. Nevertheless, the overall temperature depedence of the resistivity does not change much when J is reduced.

The structure is taken from experimental measurements and only paramagnetic state is considered. The muffin-tin radii are 2.30, 1.94 and 1.72 Bohr radius for Sr(Ca), Ru and O respectively. In the charge-self-consistent calculation, the Brillouin zone integration is performed with a regular 13x9x13, 13x9x13, 14x14x14 and 12x12x12 mesh for $SrRuO_3$,$CaRuO_3$, Sr_2RuO_4 and $Sr_3Ru_2O_7$ correspondingly. In the calculations of optical conductivity and resistivity, a mesh with typically 10000 k-points in the full Briillouin zone is adopted.

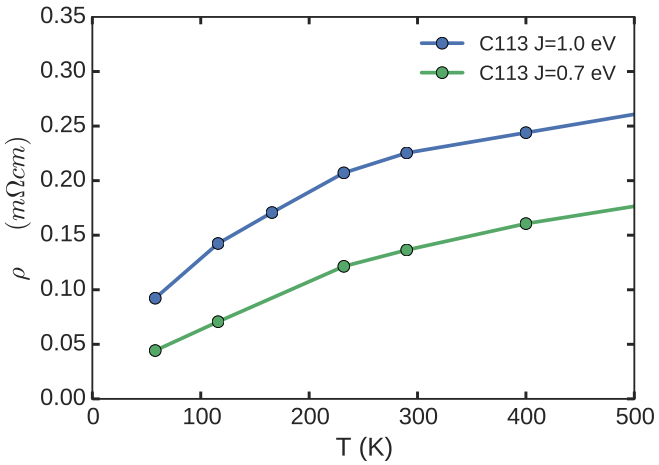

FIG. 1. The computed resistivity of $CaRuO_3$ with two different Hund's coupling J.

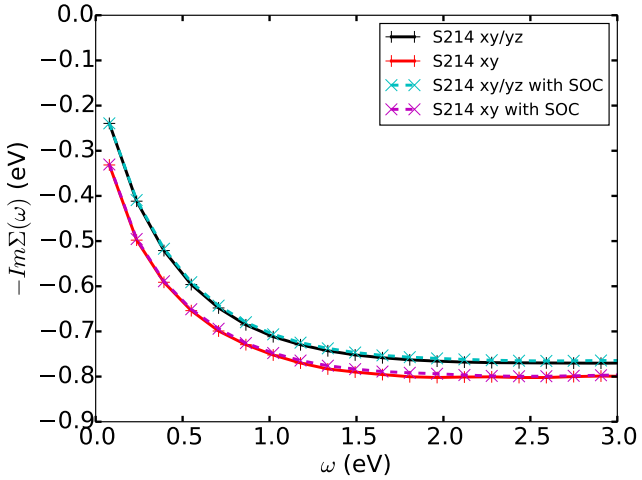

FIG. 2. The computed self energies of Sr_2RuO_4 with and without spin-orbit coupling considered in the LDA+DMFT calculations. The inverse temperature is $\beta = 1/T = 40eV^{-1}$.

To solve the impurity problem, we use continuous-time quantum Monte-Carlo method with hybridization expansion [4, 5]. After the DMFT convergence is reached, we performed a few additional iterations (typically over 10 times) to get better statistics. The self energies on real axis are obtained with the maximum entropy method. Rather than analytically continuing the self energy $\Sigma(i\omega_n)$ itself, we adopt the trick to analytically continune the auxillary Green's functions $G(i\omega_n) = 1/(i\omega_n - \Sigma(i\omega_n))$ since it is better behaved than $\Sigma(i\omega_n)$, and then extract $\Sigma(\omega)$ on real axis. The quasiparticle weight Z and self energy at zero frequency $\Sigma(0)$ are extracted from the Matsubara frequency self energy directly with polynomial fit to a few low frequency data points. We analyze the self-energies from the last few iterations to obtain an estimation of the error bars of the quasiparticle effective mass and scattering rate. We find that the typical relative error is less than 10%.

We note that spin-orbit coupling effect is not considered in our calculation scheme. Moreover we have verified that taking into account spin-orbit coupling explicitly in the LDA part has negligible effects to the self energy, as shown in Fig. 2 for an example calculation in Sr_2RuO_4.

Appendix B: Electron-phonon interaction from first principles computations

In the main text, we have only considered the electron-electron correlation in the framework of LDA+DMFT method. From the good agreement with experimental measurements we draw the conclusion that the electron-electron interaction dominates the electron scattering in ruthenates. This implies that electron-phonon interaction, another important mechanism of electron scattering, plays a minor role in ruthenates. To further support this point, we have computed in Sr_2RuO_4 the electron-phonon interaction (EPI) and the EPI-induced resistivity in the framework of Eliashberg theory from first principles . Our result confirms our expectation and shows that EPI contributes less than 5% of the total resistivity.

The calculation is made possible with the pseudopotential planewave package ABINIT[6]. We take the conventional cell with 14 atoms in total as the input structure. To evaluate the Eliashberg spectra function, integrals have to be performed over crystal momentum $\mathbf{k}$ and phonon momentum $\mathbf{q}$, which would require a very high computational cost. We try to get a reasonable estimation from a minimal setup of calculation. We sample crystal momentum $\mathbf{k}$ using a dense 12x12x4 mesh to reasonably captures the complexity of the Fermi surfaces of Sr_2RuO_4, and sample the phonon momentum $\mathbf{q}$ using a rough 2x2x1 mesh . The $\mathbf{q}$ mesh might seem too coarse. However we note that in the EPI-induced resistivity an average over $\mathbf{q}$ is involved, so a coarse mesh would be able to capture reasonably the average scattering rate due to EPI. In the calculations the norm-conserving pseudopotentials are used, the plane-wave cutoff energy is chosen to be 40eV and the local density approximation of the exchange-correlation functions is adopted. We note that the on-site electron-electron interaction is not considered in this calcualtion.

To gain some confidence with our setup, we perform a benchmark computation with similar setup in the elemental Aluminum. We use a dense 20x20x20 $\mathbf{k}$-mesh and a coarse 2x2x2 $\mathbf{q}$-mesh. The computed resistivity is shown in Fig.3(a), which is quite close to those reported in 7 as well as experiments referred therein. Therefore we believe our

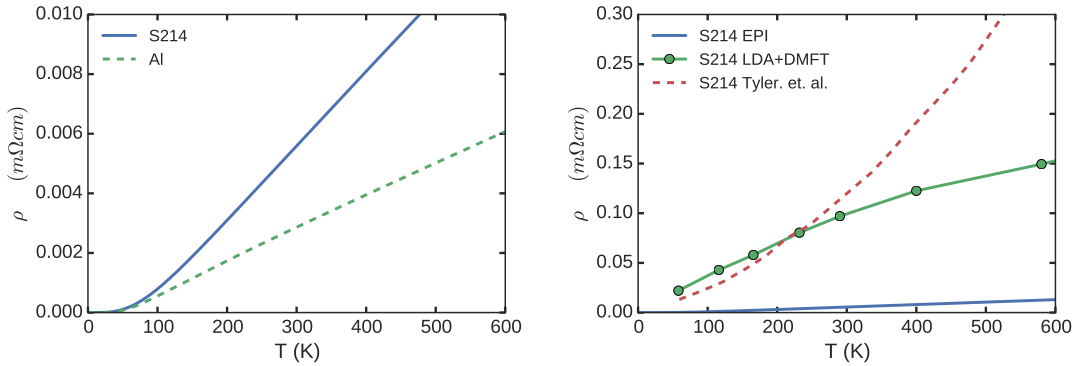

FIG. 3. The computed in-plane resistivity of Sr_2RuO_4 due to electron-phonon interaction ρ_{EPI} using ABINIT. (a) ρ_{EPI} is plotted along with with the computed resistivity of Aluminum. (b) ρ_{EPI} is plotted along with the computed resistivity in LDA+DMFT method and the measured resistivity.

setup can give a reasonable estimation of the resistivity induced by EPI.

The computed electron-phonon coupling constant λ in Sr_2RuO_4 is around 0.33. The computed in-plane resistivity induced by EPI in Sr_2RuO_4 is shown Fig.3(a). The overall scale is relatively small, close (as large as only two times) to that of the very good metal Aluminum. The EPI-induced resistivity accounts less than 5% of the total resistivity when compared to the experimental measurement, and is less than 10% of that predicted by LDA+DMFT calculation, as shown in Fig.3(b). These results demonstrate that the EPI plays a minor role in the resistivity of Sr_2RuO_4. We expect that this conclusion holds in all ruthenates considered due to the similarity in their structures.

We notice that the resistivity due to EPI can not account for the discrepancy between the experimental measurement and our LDA+DMFT calculated resistivity at high temperature (larger than 300K). This leads to the hypothesis that effects beyond our consideration, such as vertex correction and non-local interaction are important in the layered compounds. Unfortunately, so far there are no reliable techniques to estimate the contributions to the resistivity due to these two effects. Further developments and investigations are called for.

Appendix C: Hidden Fermi liquid behavior in ruthenates

We have shown that the hidden Fermi liquid behavior occurs in $CaRuO_3$ based on analysis on experimental measurements[8]. Previous LDA+DMFT calculation on $CaRuO_3$ supports our finding[9]. In the main text our results from LDA+DMFT calculations shows that in all the ruthenates the quasiparticle scattering rate complies with the hidden Fermi liquid scenario, exhibiting a parabolic temperature dependence beyond the measured Fermi liquid scale. To better illustrate this scenario, we plot the quasiparticle scattering rate of all orbitals in the ruthenates considered in Fig.4 as Γ/T versus temperature. It clearly shows that $\Gamma/T = -2ZIm\Sigma(0)/T$ of each orbital has a pronounced T-linear term in a large temperature range (up to around 200K). Therefore hidden Fermi liquid behavior is general in ruthenates. Further experimental justification would be interesting to see.

Appendix D: Weiss functions, local Green's function and the relative correlation strength and its relation to the structure parameters in ruthenates

In this section we present the Weiss functions, the local Green's functions of the localized orbitals, and the structure parameters of the ruthenates considered. We show their relations with the relative correlation strength as discussed in the main text.

The quantity characterizing the coupling between a localized orbital and its environment in dynamical mean field theory (DMFT) is the Weiss function $\Delta(\omega)$[10]. A larger imaginary part of Weiss functions at low frequency indicates a more itinerant character thus weaker correlation in the corresponding orbital. In DMFT the Weiss function is self-consistently determined, nevertheless the initial Weiss function which enters the first DMFT iteration gives useful hints of the coupling strength. The imaginary part of the initial Weiss functions for all the orbitals in ruthenates are depicted in Fig 5(a). It shows that the $d_{xz/yz}$ orbitals of Sr_2RuO_4 are special with much higher value of Weiss function near zero frequency than the other orbitals, in which the values of Weiss functions are similar if averaged

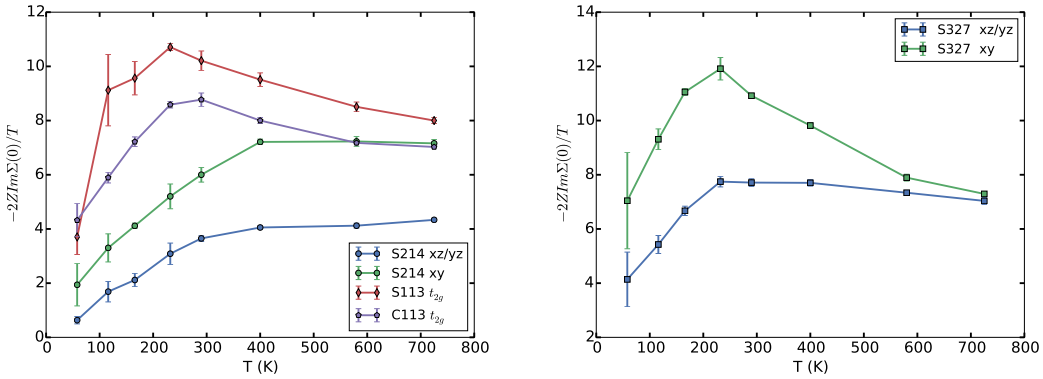

FIG. 4. The quasiparticle scattering rate over temperature for each orbital of (a) Sr_2RuO_4, $SrRuO_3$, $CaRuO_3$, and (b) $Sr_3Ru_2O_7$. The error bar is estimated from self energies of the last few converged iterations.

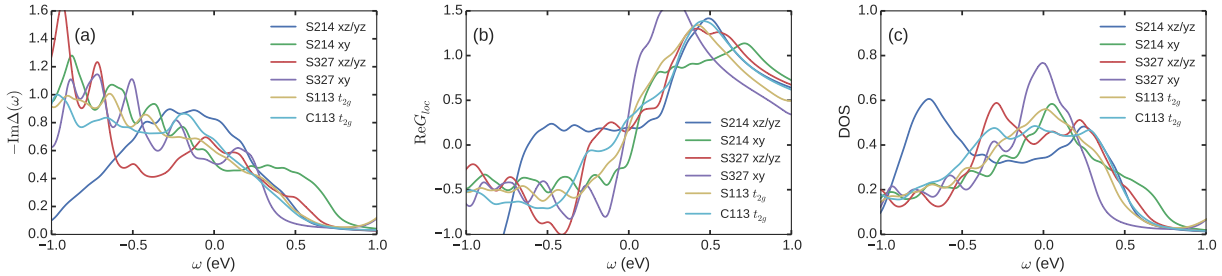

FIG. 5. The imaginary part of the Weiss function (a) entering the first DMFT iteration, the real part of local Green's functions (b) and the density of states (c) computed from DFT for all the orbitals in ruthenates considered in the main text. S113, C113, S214, S327 are acronyms for $SrRuO_3$, $CaRuO_3$, Sr_2RuO_4 and $Sr_3Ru_2O_7$.

over a smaller energy range around the Fermi level. We have checked the corresponding low frequency values of the self-consistent Weiss functions in our DMFT calculations and found similar results.

Following the same argument of Ref. [3], the initial Weiss function is the inverse of the local Green's functions computed in DFT, that is, $\mathrm{Im}\Delta(\omega) = -\mathrm{Im}G_{loc}^{-1}(\omega) \simeq \frac{1}{\mathrm{Im}G_{loc}(\omega)}$. $G_{loc}(\omega)$ is a matrix with orbital indices in multiorbital systems, and the approximation holds if $\mathrm{Re}G_{loc}$ is relatively small and the off-diagonal terms in $\mathrm{Im}G_{loc}$ are negligible. Indeed it is true that in ruthenates $\mathrm{Re}G_{loc}$ is much smaller than $\mathrm{Im}G_{loc}$ and close to zero near zero frequency as shown in Fig.5(b). $\mathrm{Im}G_{loc}$ relates to the density of states of localized orbitals $\rho_\alpha = -\frac{1}{\pi}\mathrm{Im}[G_{loc}]_{\alpha,\alpha}$. ρ_α for all the orbitals are shown in Fig.5(c). We see that the approximate inverse relation between the Weiss function and the density of states is obeyed, (d_{xy} orbital of $Sr_3Ru_2O_7$ is an exception which has a much higher density of states than the others but the Weiss function is not significantly lower possibly due to the off-diagonal terms in G_{loc}). In accordance with the large value of its Weiss function, the $d_{xz/yz}$ orbitals in Sr_2RuO_4 have the lowest density of states near the Fermi level, which explains their relative weak correlations. As discussed in the main text, this is because that these orbitals have typical one-dimension feature that a large part of their spectral weight is distributed near the band edges due to the quantum confinement along the out-of-plane direction. When going from single layered structure to the pseudocubic ones, their one-dimension nature is gradually destroyed so that their density of states near the Fermi level increase (in the end they are nearly degenerate with d_{xy} orbital), and their correlations are enhanced.

As discussed in the main text, the Weiss function can not be used to explain the relative correlation strength in the d_{xy} (t_{2g} in pseudocubic compounds) orbitals. This is demonstrated in Fig.5(a), that all these orbitals have similar value of Weiss function near zero frequency, however the d_{xy} orbital in Sr_2RuO_4 has a relative smaller effective mass enhancement and quasiparticle scattering rate (See main text). In Table.I, the experimental parameters of ruthenates including the in-plane/out-of-plane Ru-O bond length, the rotation and tilt angles of oxygen octahedra are shown along with the effective mass enhancement of d_{xy} orbital computed in DFT+DMFT. Going from single layered Sr_2RuO_4 to the psuedocubic ones, the in-plane Ru-O bond length increases and the rotation and tilting of oxygen octahedra develops, meanwhile the d_{xy} orbital becomes more correlated and acquires a larger quasiparticle mass. Therefore the relatively weak correlation strength of d_{xy} orbital in Sr_2RuO_4 is very likely related to the corresponding short in-plane Ru-O distance and the absence of rotation and tilting of oxygen octahedra. This is understandable that

larger in-plane Ru-O bond length and the rotation and tilting of oxygen octahedra make d_{xy} orbital more localized.

	d_{Ru-O} (in-plane)	d_{Ru-O} (out-of-plane)	θ_{rot}	θ_{tilt}	$m^*_{\rm theory}/m_{\rm DFT}$ (d_{xy},t_{2g})
Sr_2RuO_4	1.936	2.067	0.0	0.0	5.4
$Sr_3Ru_2O_7$	1.959	2.023	7.0	0.0	6.4
$SrRuO_3$	1.984	1.988	6.5	8.8	6.6
$CaRuO_3$	1.998	1.983	11	15	6.9

TABLE I. The structure parameters including Ru-O bond length, oxygen octahedra rotation and tilt angles are shown along with the calculated quasiparticle mass enhancement of d_{xy} (t_{2g}) orbitals of all the compounds considered in the main text. Units of bond length and angle are $\mathring{A}$ and degree respectively.

[1] K. Haule, C. Yee, and K. Kim, Physical Review B **81**, 195107 (2010).
[2] P. Blaha, K. Schwarz, G. K. H. Madsen, D. Kvasnicka, and J. Luitz, *WIEN2K, An Augmented Plane Wave + Local Orbitals Program for Calculating Crystal Properties* (Karlheinz Schwarz, Techn. Universität Wien, Austria, Wien, Austria, 2001).
[3] J. Mravlje, M. Aichhorn, T. Miyake, K. Haule, G. Kotliar, and A. Georges, Physical Review Letters **106**, 096401 (2011).
[4] K. Haule, Physical Review B **75**, 155113 (2007).
[5] P. Werner, A. Comanac, L. de' Medici, M. Troyer, and A. J. Millis, Physical Review Letters **97**, 076405 (2006).
[6] X. Gonze, B. Amadon, P. M. Anglade, J. M. Beuken, F. Bottin, P. Boulanger, F. Bruneval, D. Caliste, R. Caracas, M. Côté, T. Deutsch, L. Genovese, P. Ghosez, M. Giantomassi, S. Goedecker, D. R. Hamann, P. Hermet, F. Jollet, G. Jomard, S. Leroux, M. Mancini, S. Mazevet, M. J. T. Oliveira, G. Onida, Y. Pouillon, T. Rangel, G. M. Rignanese, D. Sangalli, R. Shaltaf, M. Torrent, M. J. Verstraete, G. Zerah, and J. W. Zwanziger, Computer Physics Communications 40 YEARS OF CPC: A celebratory issue focused on quality software for high performance, grid and novel computing architectures, **180**, 2582 (2009).
[7] S. Y. Savrasov and D. Y. Savrasov, Physical Review B **54**, 16487 (1996).
[8] X. Deng, A. Sternbach, K. Haule, D. N. Basov, and G. Kotliar, Physical Review Letters **113**, 246404 (2014).
[9] H. T. Dang, J. Mravlje, A. Georges, and A. J. Millis, Physical Review B **91**, 195149 (2015).
[10] A. Georges, G. Kotliar, W. Krauth, and M. J. Rozenberg, Reviews of Modern Physics **68**, 13 (1996).